Egypt. J. Chem. **Vol. 65,** No. 2 pp. 459 - 469 (2022)

Egyptian Journal of Chemistry

http://ejchem.journals.ekb.eg/

Petrogenesis of chemical compositional trends within a mafic dyke at Wadi Lethi, Southern Sinai, Egypt.

Abd El Ghaffar, N.I.

Geological Sciences Department, National Research Centre, Dokki, 12622 Cairo, Egypt

Abstract

Systematic mineralogical and chemical composition variations across a mafic dyke at the Wadi Lethi area, in southern Sinai, are observed. This dyke extrudes the Neoproterozoic Younger Granite of southern Sinai. New petrographic, geochemical data, and mineral chemistry data are applied to predict the evolution scheme of this dyke. The collected samples vary in composition from (outward zone) basalt to (inward zone) andesite. The studied samples exhibit a wide uniform variation in main oxides and trace elements content and display a significant inward chemical variation.

The studied samples are mainly identified into (basalt, basaltic-andesite, trachy-andesite, and andesite). The geochemical characters reveal that the investigated dyke originated from calc-alkaline magma under orogenic tectonic setting. Mineral chemistry data reveals that the studied dyke formed at water pressure ranges from 1-3 kbr and low oxygen fugacity conditions. The fractional crystallization process is assumed to have prevailed during the extrusion of the investigated dyke.

Keywords: Mafic dyke, mineral chemistry, petrogenesis, zonation

1. Introduction

The significant interface between many of the extrusive dykes and their hosting granitic plutons is usually attributed magma generation along with joint-like fractures [1, 2]. The Neoproterozoic cratonization of Sinai massif and the Eastern Desert of Egypt was accompanied by extensive granitic plutonism followed by several episodes of crustal extension and dykes emplacement. Akaad and [3-6]. stated that the dykes in the basement complex of Egypt display a transitional time from compressional to extensional orogenic regime, and their origin is depending on lithospheric dynamics (passive rifting) and not by the asthenosphere rise (active rifting). These dykes are chronologically classified as post granite dykes. Geochronologically, three mechanisms of dykes generation have been discriminated in the Egyptian basement rocks, (1) metamorphosed syn-tectonic dykes (800–650Ma; [7], (2) non-metamorphosed post-tectonic dykes (591–459 Ma; [8]; [9-13] and (3) Neogene dykes (30–12 Ma; [14-15] related to the updoming and opening of the Red Sea Rift system. The first two categories are represented by mafic to felsic dykes, whereas the third category dykes are mafic in composition. In Sinai, various dyke types of Pan-African age [16-17] and Tertiary dykes [18] have been identified. Although the enrichment of the dykes extruding the basement complex of the NW domain in Sinai, only little literatures about dykes are available.

Generally, zonation includes two features (normal zonation and reverse zonation), normal zonation is rare and reverse zonation is common. The mechanism of such zoning is quite different, four main mechanisms are responsible for reverse zonation [19], 1- Magma contamination, 2- flow differentiation, 3- In situ crystal growth on the walls of the dyke, and 4- Compositional change of the emplaced magma, in contrast, fractional crystallization of magma is the main cause of normal zonation.

In the present work, an internal compositional variation (zonation) is observed in a mafic dyke extruded the Younger Granite of Wadi Lethi area. These phenomena are important to predict the emplacement conditions controlling the extrusion of this dyke. Application of new data (petrography, geochemistry, and mineral chemistry data) during the studying of this dyke to assess the extrusion conditions of this dyke.

2. Geology of the investigated area

Wadi Lethi area (Fig. 1) is located between Lat. 27° 50-28° 27' 59" and long 33° 55' -34° 15' and covers an area of about 10 km2 in the west of the

*Corresponding author e-mail: nahla169@yahoo.com.; (Tel: +201003801148).
Receive Date: 02 August 2021, Revise Date: 23 August 2021, Accept Date: 25 August 2021
DOI: 10.21608/EJCHEM.2021.88960.4271

Sharm El-Sheikh Mountains, South Sinai. The area is accessible through an asphaltic road (Sharm-Dahab). The geomorphology of the considered area depends on the rock types and the main structures. Generally, the investigated area is occupied by moderate to high elevated mountains. The area is mainly occupied by granitoid rocks belonging to the Neoproterozoic rocks of the northern domain of the Arabian-Nubian Shield which is related to the calc-alkaline phase of the youngest magmatic activity of the Arabo-Nubian Shield [20] The sequence of the basement rocks exposed in the studied area from oldest to youngest is as follows: 1- Metavolcanics, 2- Older granite (Diorite-Tonalite- Granodiorite) 3- Dokhan volcanics, and 4- Younger granite phase- III (Alkaline granite) following [21].

The basement rocks at the Wadi Lethi area are strongly affected by a system of NNE trending faults. Several acidic, intermediate, and basic dykes cut these rocks. These dykes vary in their distribution, trends, morphology, and petrographic characteristics. The basic and intermediate dykes are predominant while the other types are relatively subordinate. Most of these dykes relatively tolerate weathering giving high ridges relative to their country rocks. They cut across the hosts (Younger Granite) and usually have sharp contacts. Branching of dykes is frequently observed. These dykes usually exhibit a marked variation in color, grain size, texture, and composition. They are usually devoid of enclaves from the host rocks. These dykes vary in length and width and variably form swarms running parallel to each other. The majority of dykes' trends are NE-SW, NNW-SSE, and NW-SE. Generally, the dykes are fine to medium-grained, massive, and sometimes show porphyritic texture. There is an intersection relationship among variable types of dykes. The investigated dyke is of 3.5 m thick and may extend over 300 m in length with NE-SE trend (Fig. 2).

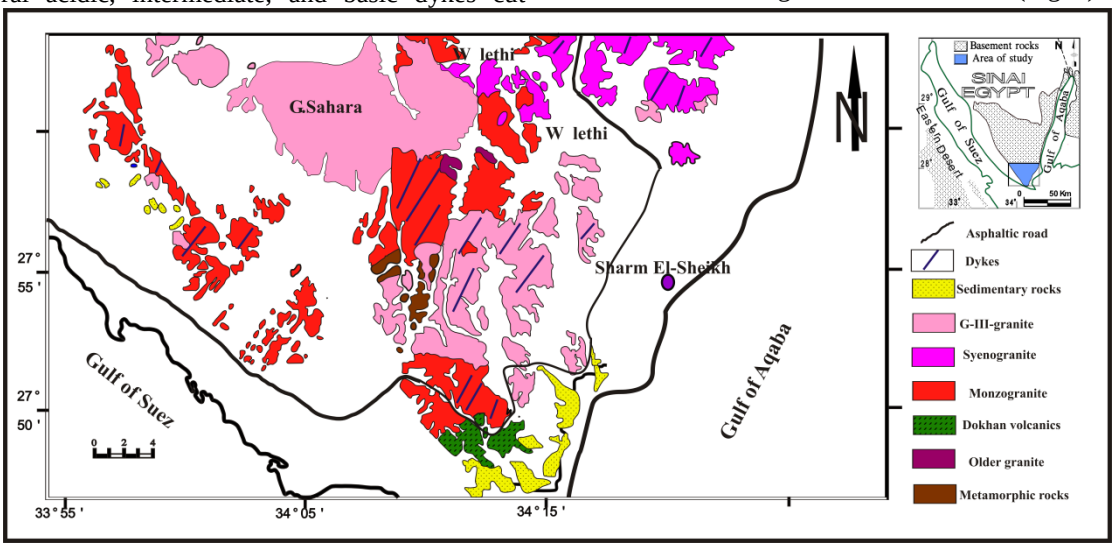

Fig. 1. Geological map of the studied area.

Fig.2. Field photo of the studied dyke extruded the Younger Granite (YG).

2.Result and discussions

2.1. Petrography

Petrographical investigation reveals that the margins of the investigated dyke are basaltic in composition and grade inward into an andesitic composition.

Basalt

The investigated basaltic samples are commonly equigranular and made of plagioclase ranging in composition from labradorite to andesine ($An_{45–65}$), augite, and hornblende (Fig.3A). Epidotes, chlorite, tremolite-actinolite, and, iron oxides (Fig.3B) are the main alteration products. Moderate kaolinization and sassuritization are recorded. Lathes are variably arranged intergranular texture (Fig. 3C). Oscillatory zoning is variably recorded (Fig. 3D).

Andesite

Andesitic samples are composed of plagioclase, hornblende, biotite with subordinate k feldspar, and quartz. Titanite, allanite, apatite, and opaques are the accessory phases (Figs. 3E&F). Epidote, kaolinite, tremolite- actinolite, and chlorite are the alteration products. Plagioclase (An30–42) is a common phase; represented by subhedral crystals Partial alteration of some crystals to kaolinite is variably observed. Hornblende forms subhedral elongated crystals associated with biotite. Biotite exists as clustered flakes partly altered to chlorite and iron oxides (Fig. 3G). Quartz is rare and exists as cracked crystals with undulated extinction. Quartz-k feldspar intergrowth is recorded (Fig.3H).

2.2. Mineral chemistry

Representative chemical analyses of some essential minerals (Feldspar represented by plagioclase, hornblende, biotite, and chlorite) from the investigated samples were estimated by electron microprobe and displayed in Tables 1,2 and 3. at the University of Nevada in Las Vegas (U.S.A).

The Plagioclase chemical formula was computed following (8) oxygen atoms using Minpet software after [22]. Plagioclase composition ranges from oligoclase, andesine to babradorite reaches (Ab23.2-75 & An62-23.2). The classification of plagioclase following the postulated nomenclature ternary plot after [23] is exhibited in Fig.4.

Amphibole minerals are represented by hornblende as the most common essential mafic phase. The discrimination and classification following [23] are displayed in Figs. 5&6. The wide composition of plagioclase supports the fractional crystallization trend.

The chemical analyses of hornblende are listed in Table 2. The cations number of hornblende was calculated on the basis of (23) oxygens. Z, Y, X, and A sites in the hornblende follow the empirical formula of A0-1 X2-3 Y5 Z8 O22 (OH, F, Cl)2 after [25]. Following [26], the studied samples are fall in the calcic amphibole field. Further subdivision of the amphiboles according to the plot Mg/ (Mg+Fe2+) against TSi is given in Fig. 6 which indicates that most of the analyzed samples are fall in tschermakite (Ca-rich amphibole), Tsch-Hbl and less extend to Magnesio-hornblende following [26].

Following the hornblende chemical analyses, the studied rocks have formed under low oxygen fugacity (fO2) conditions according to the relation postulated by [27] (Fig.7). According to the diagram Fe/(Fe+Mg) versus AlIV+ AlVI of [28], The amphiboles in study samples are mostly plotted in the field 1-3 kbar (Fig. 8).

Chemical compositions of biotites are listed in Table 3. The chemical formula was computed according to (24) oxygen atoms and ignoring H2O using Minpet Software after [22]. Accordingly, the chemical analyses of biotite crystals are fall within the lepidomelane field (Fig.9).

Chemical analyses of chlorite are listed in Table 4. The chemical formula was calculated following (24) oxygen accordingly; the chemical compositions of chlorite are mainly chamosite (Fe rich chlorite) (Fig. 10) adapted to [29].

2.3. Geochemistry

The collected fresh samples are chemically analyzed for major oxides and minor elements by XRF in Acme Lab. LTD., (Vancouver, Canada).

The selected chemical analyses of the collected samples are displayed in Table 5. The studied dyke exhibits a wide uniform variation in major oxides and minor elements and displays a significant inward chemical variation. SiO2 contents ranges from 51.39 % to 61.75 %, Al2O3 (18.09%-14.76%).The studied samples have a high abundance of Fe2O3 and MgO. Generally, the studied samples exhibit an inward increase of SiO2, TiO2, Na2O against a decrease in MgO and Fe2O3 that support a normally closed system (fractionation of basaltic magma). Binary variation plots between MgO and major oxides are displayed in Figure 11, the studied samples display normal fractional crystallization trends.

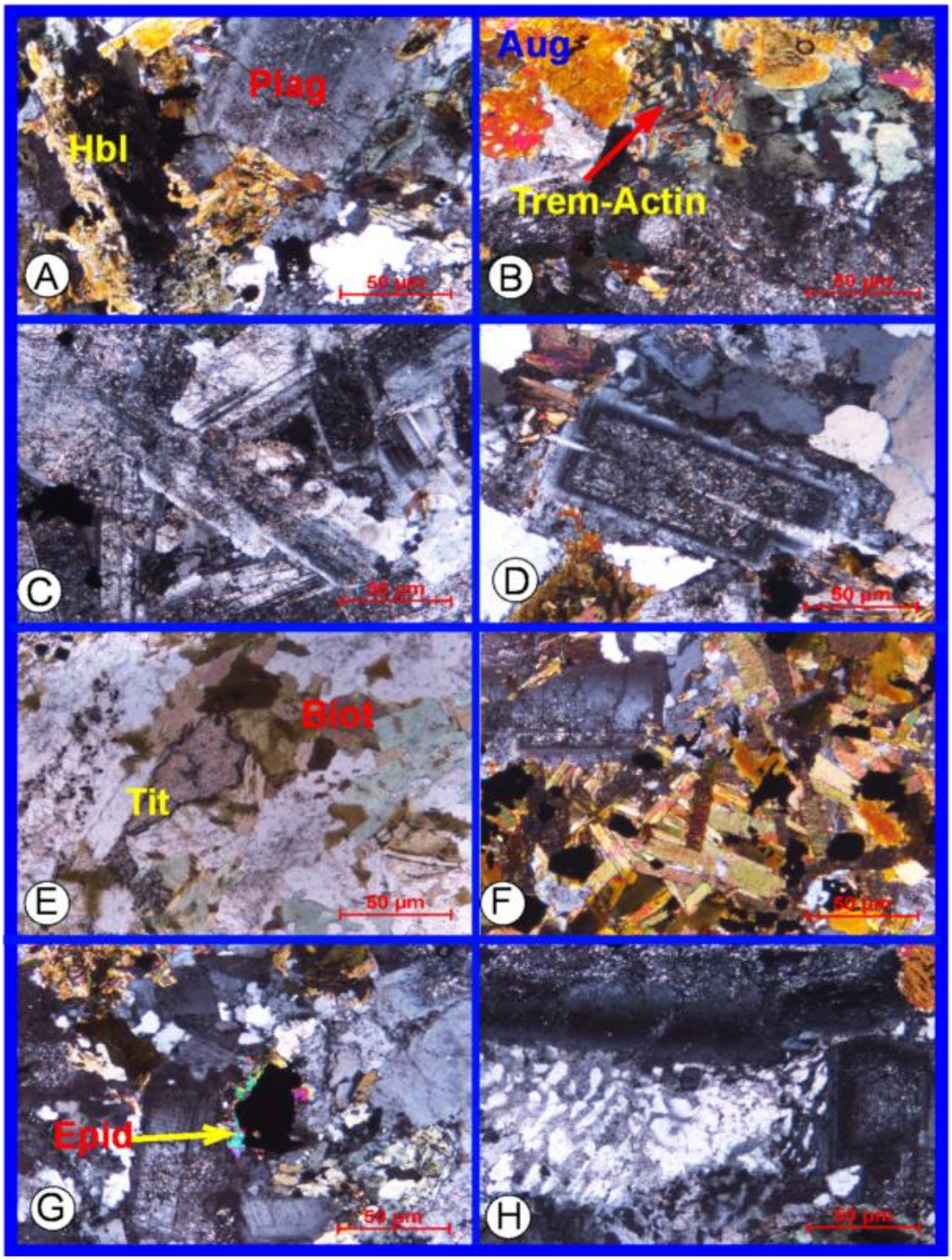

Fig.3. Microphotographs displaying: A. simply twinned hornblende and plagioclase crystals, B. Alteration of augite (Aug) to tremolite and actinolite (Trem-Actin). C- Plagioclase lathes display intergranular texture. D- Oscillatory zoned plagioclase crystal. E. Association of biotite (Biot) and titanite (Tit) crystals. F. Association of biotite flakes with opaques. G. Opaque crystal rimmed by epidote. H. Graphic intergrowth of quartz and k feldspar.

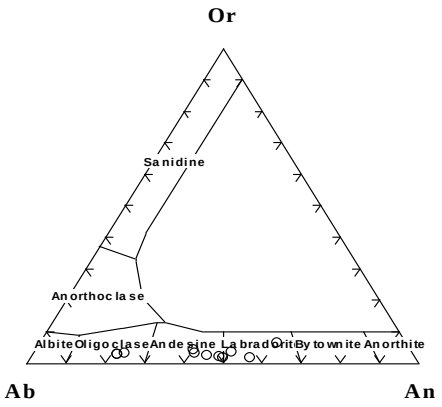

Fig.4. Plagioclase chemistry on the Or-Ab-An plot.

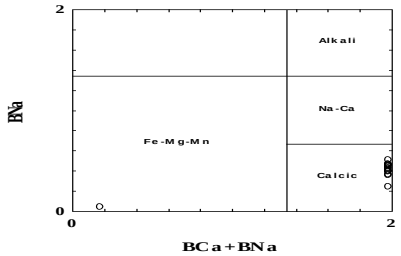

Fig.5. Amphibole classification plot.

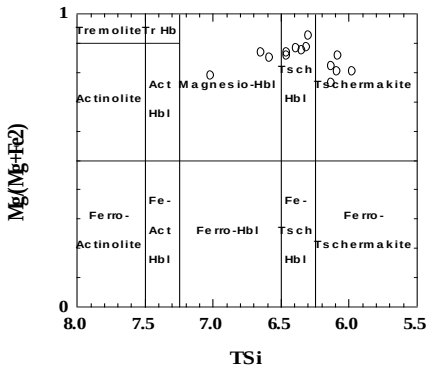

Fig. 6. Hornblende classification plot.

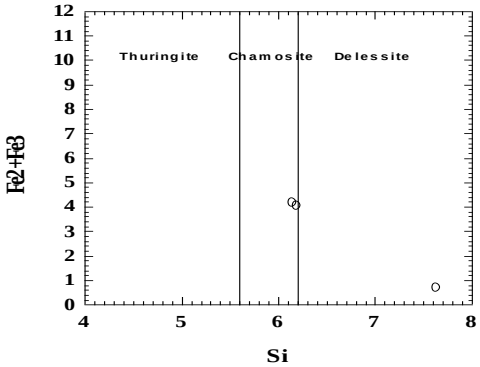

Fig.10.Chlorite classification plot

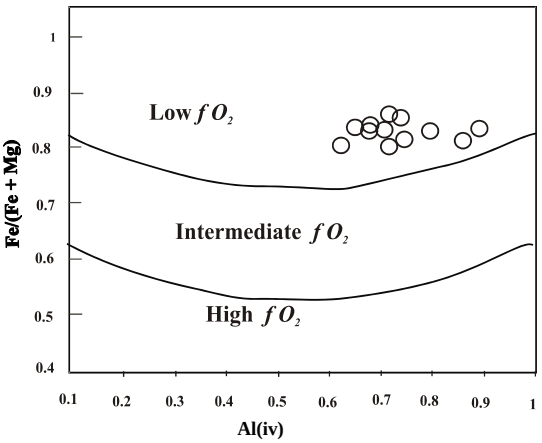

Fig.7. Plot of [27] using the chemical analyses of hornblende in the studied samples.

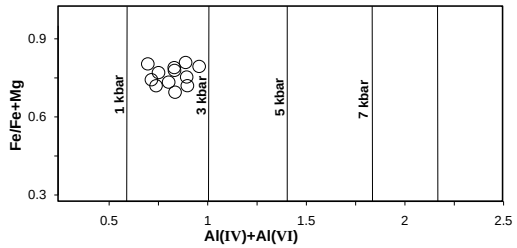

Fig.8.Plot of Fe/(Fe+Mg) *vs* Al(IV)+Al(VI) for hornblende from the studied samples.

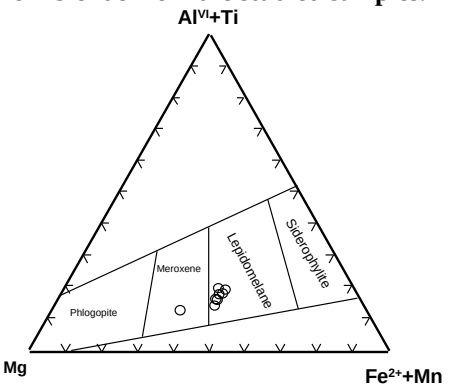

Fig.9. (Al^{VI}+Ti)-Mg-(Fe^{2+}+Mn) classification diagram for the analyzed biotite .

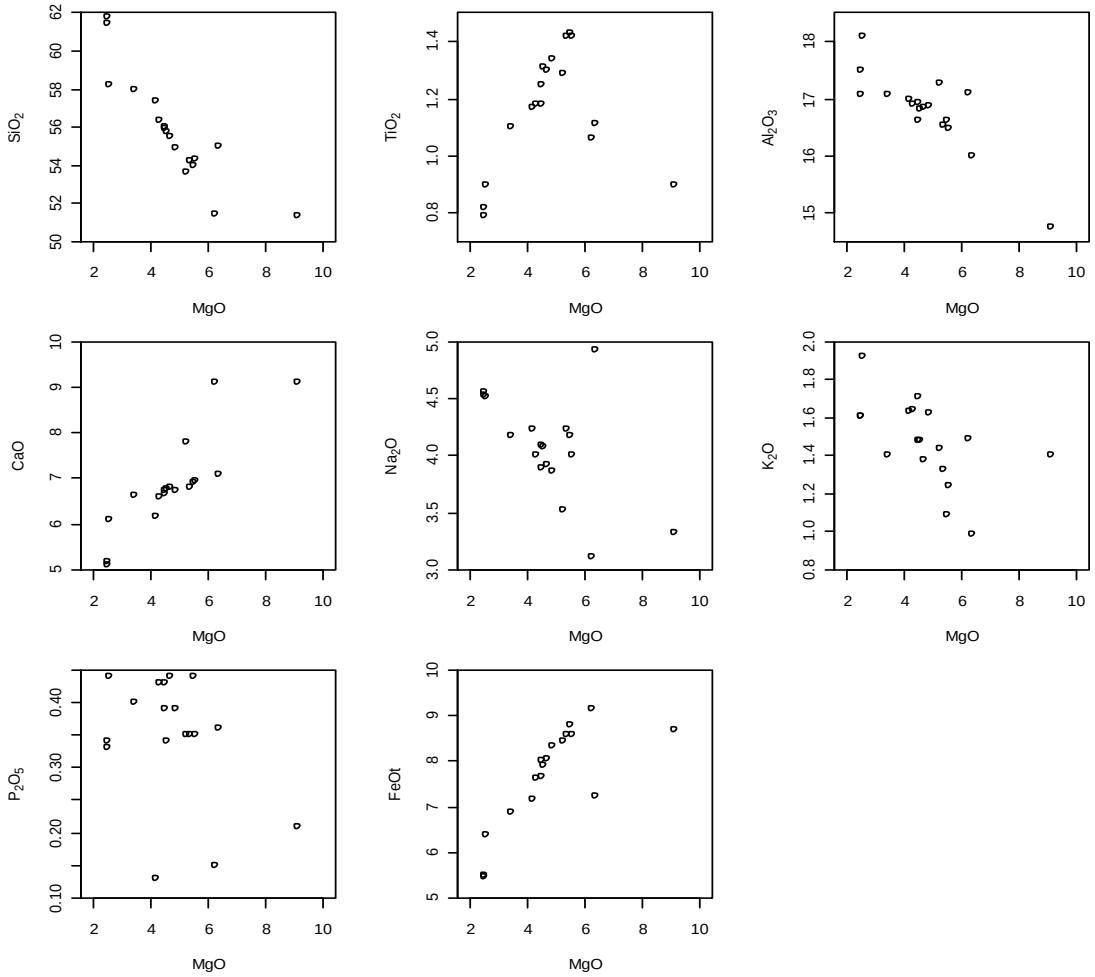

Fig.11. Binary variation plots of major oxides versus MgO.

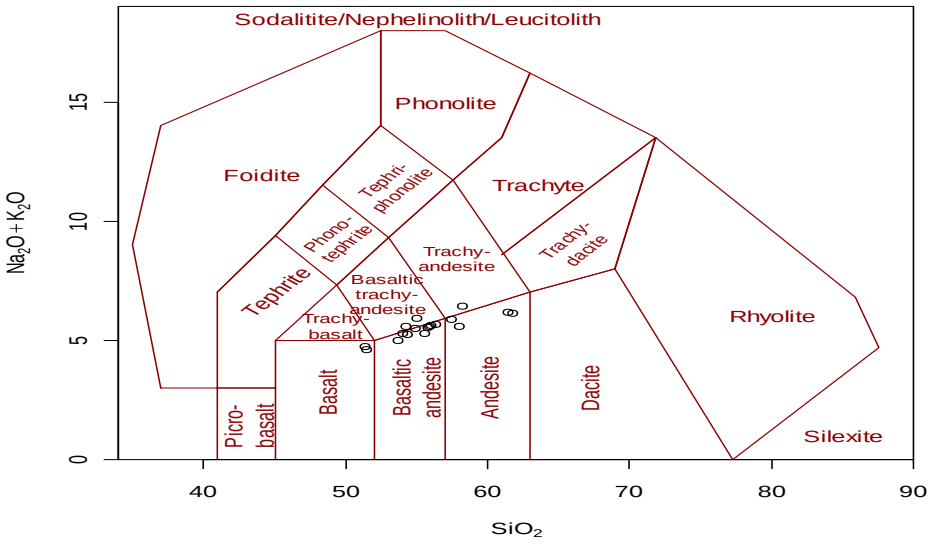

Fig. 12. Geochemical classification diagrams of Middlemost for volcanic rocks.

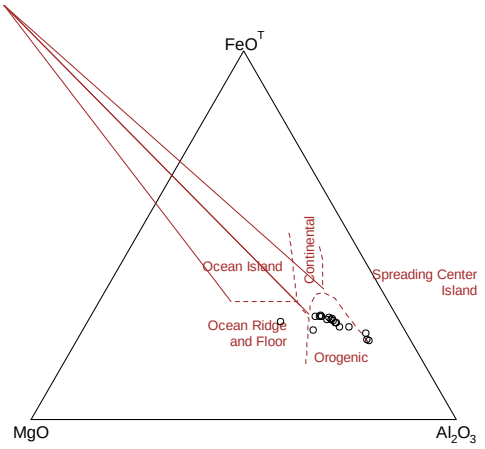

Fig. 13. Ternary diagrams of [31] for the studied rocks

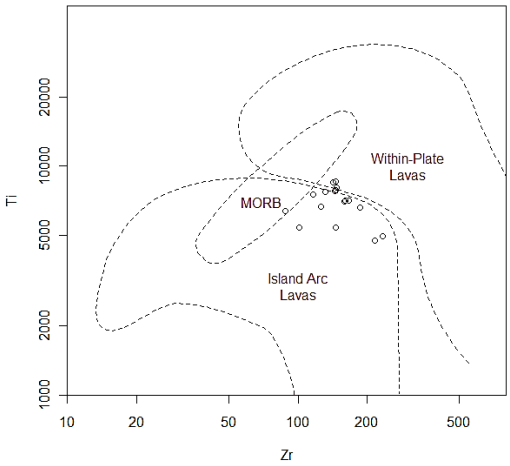

Fig. 14. The studied sample on the binary diagrams of [32].

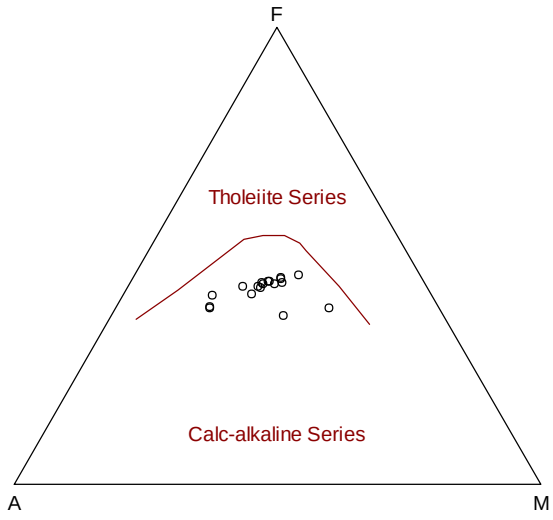

Fig.15. The studied sample on AFM diagram of [33].

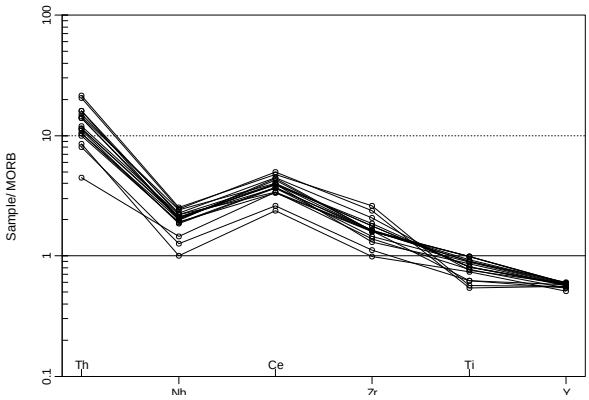

Fig.16. Spider plot of the studied samples according to MORB of [34].

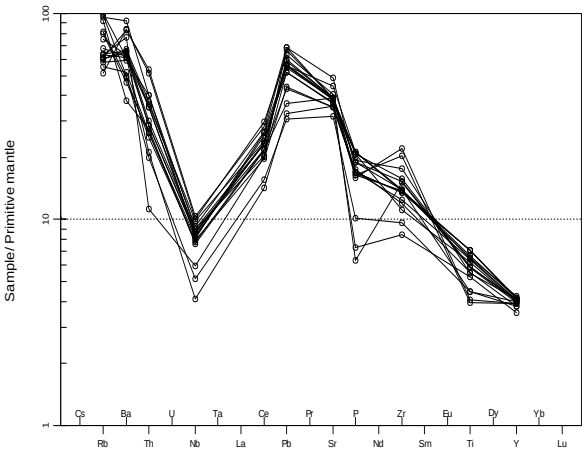

Fig.17. Spider plot of the studied samples according to primitive mantle of [35].

According to the plot of [30], the studied samples are mainly classified into trachy-andesite, basaltic andesite, andesite, and basalt (Fig.12). Following the ternary plot of [31] the studied samples are fall in the orgenic field (Fig.13). On the Zr-Ti binary plot of [32], the studied samples are mainly plotted in island arc lavas and extend to within plate lavas (Fig.14). The AFM ternary plot of [33] reveals that the investigated samples are wholly plotted in the calc-alkaline series (Fig 15).

Elements abundant diagrams (Figs.16&17), in which concentrations are normalized to the hypothetical Mid Oceanic Ridge basalt composition [34] and primitive mantle composition [35], may give a general indication of the source and tectonic affinities of studied samples. The concentration of LILE is significantly higher (Cs, Rb, Ba, and Sr) against HFSE (Nb, Zr, Y, Ti, and Ce) with a negative Nb anomaly. The depletion of Nb and Ti could be attributed to titanite- ilmenite fractionation [36]. Positive Zr anomaly suggests crustal contamination processes [37]. A wide range of major oxides and higher content of LILE support post magmatic processes affected the composition of the investigated dyke [38].

Table. 1. Selected chemical analyses of plagioclase feldspar from the studied dyke.

Sample	plg-1	plg-10	plg-11	plg-2	plg-3	plg-4	plg-5	plg-6	plg-7	plg-8	plg-9
SiO_2	61.44	60.9	54.55	60.78	55.35	50.54	56.1	52.44	53.93	56.6	53.44
TiO_2	0.03	--	--	0.01	--	0.05	0.02	0.03	0.02	--	0.02
Al_2O_3	23.24	22.9	27.73	23.52	27.16	30.1	25.95	28.67	27.87	26.7	28.79
FeO	0.14	0.1	0.1	0.09	0.11	0.4	0.3	0.41	0.18	0.14	0.12
MnO	0.02	--	--	--	--	0.01	--	--	0.02	--	0.02
MgO	0.02	0.01	0.01	0.02	0.09	0.11	0.15	0.01	0.02	0.01	0.02
CaO	4.68	4.65	10.15	5.06	9.1	12.41	8.7	11.56	10.22	8.5	10.6
Na_2O	8.36	8.3	5.6	8.17	5.69	3.6	6.22	4.6	5.39	6.1	5.1
K_2O	0.31	0.3	0.15	0.35	0.2	0.93	0.35	0.12	0.13	0.5	0.44
Cations											
Si	5.535	5.545	5.004	5.496	5.07	4.702	5.179	4.867	4.973	5.143	4.895
Al	2.466	2.455	2.996	2.504	2.93	3.298	2.821	3.133	3.027	2.857	3.105
Ti	0.002	0	0	0.001	0	0.003	0.001	0.002	0.001	--	0.001
Fe^{+2}	0.011	0.008	0.008	0.007	0.008	0.031	0.023	0.032	0.014	0.011	0.009
Mn	0.002	--	--	--	--	0.001	--	--	0.002	--	0.002
Mg	0.003	0.001	0.001	0.003	0.012	0.015	0.021	0.001	0.003	0.001	0.003
Ca	0.452	0.454	0.998	0.49	0.893	1.237	0.861	1.149	1.01	0.827	1.04
Na	1.46	1.465	0.996	1.432	1.011	0.649	1.113	0.828	0.964	1.075	0.906
K	0.036	0.035	0.018	0.04	0.023	0.11	0.041	0.014	0.015	0.058	0.051
Ab	74.9	75	49.5	73	52.5	32.5	55.2	41.6	48.5	54.8	45.4
An	23.2	23.2	49.6	25	46.3	62	42.7	57.7	50.8	42.2	52.1
Or	1.8	1.8	0.9	2	1.2	5.5	2	0.7	0.8	3	2.6

3. Table. 2. Selected chemical analyses of hornblende fom the studied dyke.

Sample	hbl-1	hbl-10	hbl-11	hbl-12	hbl-13	hbl-14	hbl-15	hbl-2	hbl-3	hbl-4	hbl-5	hbl-6	hbl-7	hbl-8	hbl-9
SiO_2	40.99	45.15	43.53	43.45	43.12	43.25	40.93	41.29	48.17	41.55	31.9	40.08	43.88	44.38	45.49
TiO_2	2.35	1.4	1.9	2.3	2.7	2.2	2.6	2.02	0.98	2.34	2.2	3.5	2.2	1.9	1.45
Al_2O_3	10.78	8.81	9.98	9.91	10.09	10.22	10.58	11.149	6.03	10.41	15.26	9.96	8.7	9.29	8.65
FeO	18.243	15.2	15.12	15.37	14.66	15.58	18.48	18.29	14.4	18.65	21.24	19.58	15.6	15.37	13.9
Cr_2O_3	0.0012	--	--	--	--	0.03	--	0.003	--	--	0.09	--	--	--	--
MnO	0.75	0.31	0.33	0.37	0.35	0.35	0.77	0.75	0.75	0.73	0.48	0.82	0.38	0.34	0.34
MgO	9.96	12.43	11.57	11.74	11.77	11.45	9.7	10.17	13.55	10.02	15.75	9.98	11.99	12.2	12.7
CaO	11.23	12.11	12.05	11.99	11.83	12	11.65	11.43	12.11	11.65	1.03	11.2	11.93	11.96	12.26
Na_2O	1.31	1.19	1.5	1.43	1.73	1.57	1.5	1.56	0.8	1.53	0.07	1.42	1.31	1.36	1.23
K_2O	1.14	0.53	0.57	0.5	0.49	0.56	0.82	0.71	0.5	0.76	2.4	0.79	0.47	0.52	0.49
Cations															
Si	6.102	6.552	6.358	6.319	6.27	6.283	6.061	6.054	6.987	6.1	5.064	5.944	6.431	6.43	6.616
Al	1.89	1.448	1.642	1.681	1.728	1.717	1.845	1.925	1.013	1.8	2.853	1.74	1.502	1.57	1.384
Fe^{+3}	0.008	0	0	0	0.003	0	0.095	0.021	0	0.1	0.083	0.316	0.067	0	0
Al	0	0.058	0.074	0.016	0	0.031	0	0	0.017	0	0	0	0	0.015	0.098
Fe^{+3}	1.533	1.321	1.469	1.472	1.537	1.541	1.636	1.811	0.914	1.676	1.934	1.534	1.368	1.427	1.225
Ti	0.263	0.153	0.209	0.252	0.295	0.24	0.29	0.223	0.107	0.258	0.263	0.39	0.243	0.207	0.159
Mg	2.21	2.689	2.519	2.545	2.551	2.48	2.141	2.223	2.93	2.193	2.792	2.206	2.62	2.635	2.754
$Fe^{+}2$	0.729	0.523	0.377	0.398	0.243	0.352	0.558	0.411	0.832	0.513	0	0.578	0.477	0.436	0.466
Mn	0.095	0.038	0.041	0.046	0.043	0.043	0.097	0.093	0.092	0.091	0	0.103	0.047	0.042	0.042
Ca	0.169	0.218	0.31	0.272	0.331	0.31	0.279	0.239	0.107	0.268	0	0.188	0.246	0.239	0.257
Ca	1.622	1.665	1.575	1.597	1.512	1.558	1.569	1.556	1.775	1.564	0.175	1.592	1.628	1.618	1.653
Na	0.378	0.335	0.425	0.403	0.488	0.442	0.431	0.444	0.225	0.436	0.022	0.408	0.372	0.382	0.347
K	0.216	0.098	0.106	0.093	0.091	0.104	0.155	0.133	0.093	0.142	0.486	0.149	0.088	0.096	0.091

4. Table. 3. Selected chemical analyses of biotite from the studied dyke.

Sample	bio-1	bio-2	bio-3	bio-4
SiO_2	40.99	41.29	48.17	41.55
TiO_2	2.35	2.02	0.98	2.34
$Al2O_3$	10.78	11.149	6.03	10.41
Cr_2O_3	0.0012	0.003	0	0
FeO	18.243	18.29	14.4	18.65
MnO	0.75	0.75	0.75	0.73
MgO	9.96	10.17	13.55	10.02
CaO	11.23	11.43	12.11	11.65
Na_2O	1.31	1.56	0.8	1.53
K_2O	1.14	0.71	0.5	0.76
Cations				
Si	6.657	6.642	7.587	6.707
A^{IIV}	1.343	1.358	0.413	1.293
Al^{VI}	0.719	0.754	0.706	0.686
Ti	0.287	0.244	0.116	0.284
Fe^{+2}	2.478	2.461	1.897	2.518
Mn	0.103	0.102	0.1	0.1
Mg	2.412	2.439	3.182	2.411
Ca	1.954	1.97	2.044	2.015
Na	0.413	0.487	0.244	0.479
K	0.236	0.146	0.1	0.157
Fe^{2+}/Fe^{2+} +Mg	0.51	0.5	0.37	0.51
Mg#	0.49	0.5	0.63	0.49

5. Table. 4. Selected chemical analyses of secondary chlorite from the studied dyke.

Sample	chl-1	chl-2	chl-3
SiO_2	29.8	29.55	28.9
TiO_2	1.1	0.68	0.8
Al_2O_3	16.47	16.86	16.5
Cr_2O_3	0.17	0.19	--
FeO	2.65	22.1	22.57
MnO	0.29	0.3	0.63
MgO	16.79	17.4	16.84
CaO	0.18	0.2	0.76
Na_2O	0.03	0	0.04
K_2O	1.2	0.7	0.3
Cations			
Si	7.675	6.238	6.185
Al^{IV}	0.325	1.762	1.815
Al^{VI}	4.67	2.429	2.344
Ti	0.213	0.108	0.129
Fe^{+2}	0.571	3.902	4.04
Cr	0.035	0.032	0
Mn	0.063	0.054	0.114
Mg	6.446	5.476	5.373
Ca	0.05	0.045	0.174
Na	0.015	0	0.017
K	0.394	0.189	0.082
Fe^{2+}/Fe^{2+} +Mg	0.08	0.42	0.43
Mg#	0.92	0.58	0.57

6. Table. 5. Selected chemical analysis of some samples of the studied dyke.

Samples	Dl-1	Dl-2	Dl-3	Dl-4	Dl-5	Dl-6	Dl-7	Dl-8	Dl-9	Dl-10	Dl-12	Dl-13	Dl-14	Dl-15	Dl-16	Dl-17	Dl-18	Dl-19
SiO_2	51.39	54.27	54.3	55.01	53.62	53.96	55.55	55.94	56.34	54.94	57.39	57.99	58.2	61.75	61.45	55.78	51.46	56.05
TiO_2	0.9	1.42	1.42	1.11	1.29	1.43	1.3	1.25	1.18	1.34	1.17	1.1	0.9	0.82	0.79	1.31	1.06	1.18
Al_2O_3	14.76	16.54	16.48	16	17.27	16.61	16.86	16.63	16.91	16.88	17	17.07	18.09	17.06	17.49	16.81	17.1	16.94
Fe_2O_3	9.64	9.51	9.54	8.02	9.38	9.78	8.92	8.9	8.45	9.25	7.96	7.66	7.09	6.1	6.06	8.78	10.16	8.5
MnO	0.15	0.13	0.13	0.14	0.11	0.11	0.12	0.12	0.11	0.12	0.11	0.12	0.11	0.1	0.1	0.12	0.14	0.13
MgO	9.11	5.4	5.58	6.36	5.22	5.52	4.71	4.5	4.34	4.88	4.19	3.46	2.6	2.53	2.51	4.55	6.23	4.48
CaO	9.09	6.81	6.95	7.09	7.78	6.9	6.8	6.65	6.59	6.73	6.18	6.64	6.11	5.17	5.09	6.76	9.11	6.74
Na_2O	3.33	4.23	4.01	4.92	3.53	4.17	3.92	4.09	4.01	3.86	4.23	4.17	4.52	4.53	4.55	4.07	3.11	3.89
K_2O	1.4	1.33	1.24	0.99	1.44	1.09	1.38	1.48	1.64	1.62	1.63	1.4	1.92	1.61	1.61	1.48	1.49	1.71
P_2O_5	0.21	0.35	0.35	0.36	0.35	0.44	0.44	0.43	0.43	0.39	0.13	0.4	0.44	0.33	0.34	0.34	0.15	0.39
Minor Elements																		
Ce	26.2	33.1	36.9	33.9	36.4	42.8	39.4	39.5	38.9	36.7	40.4	44.7	44.2	47.3	49.8	34	23.8	39.4
Cr	1002.6	225.9	237.7	240.2	220	203.6	162.8	141.2	130.6	164.1	115.5	48.2	17.8	16.4	13.4	158.1	268.2	147
Nb	3.4	5.2	5.1	3.9	5	5.4	5.5	5.9	5.7	5.7	6.5	6.1	5.3	6.8	6.6	5.9	2.7	5.6
Ni	209.6	68.2	71	154	62.4	63.5	50.9	47.9	43.8	49.8	35.5	18.7	8.4	6.5	6.7	48.5	82.4	48.2
Pb	4.6	6.6	6.5	10.3	5.5	7.8	8.2	8.4	9	8.8	8.5	10	8.4	10.3	9.5	7.8	4.9	8.5
Rb	58.7	48.9	48.2	37.8	55.4	33.2	38	36.2	38.2	36.5	45.2	35.9	57.5	36.6	30.7	35	59.9	40.9
Sr	630.6	702.8	701.5	975.1	776.5	740	764.4	756.2	777.5	771.6	772.9	774.4	882.5	769	808.9	728.6	704.4	769.4
Th	1.6	2	2.1	0.9	2.2	2.1	2.8	2.4	2.8	2.3	2.9	3	3.2	4.3	4.1	3.2	1.7	2.3
Y	16.2	17.9	17.8	16.3	17.3	17.6	17.5	17.1	17.5	17.8	17	17.6	17.2	16.8	16.7	18.2	15.2	17.3
Zr	101.1	142.5	142.2	125.3	131.2	145.3	144.7	116.8	165.8	146.6	158.4	185.7	145.9	233.4	215.2	145.7	88.5	159.9
Ba	329.2	322.7	306.7	506.7	250.6	344.2	404.4	430.2	435	425.2	414.7	442.6	607.4	547.2	553	393.6	403.8	407.1
CIPW-norms																		
Q	0.0	4.9	5.9	2.0	6.1	5.5	8.5	8.4	8.8	7.2	9.0	11.5	9.7	15.8	15.2	7.9	2.7	8.4
Or	8.3	7.9	7.3	5.9	8.5	6.4	8.2	8.7	9.7	9.6	9.6	8.3	11.3	9.5	9.5	8.7	8.8	10.1
Ab	28.2	35.8	33.9	41.6	29.9	35.3	33.2	34.6	33.9	32.7	35.8	35.3	38.2	38.3	38.5	34.4	26.3	32.9
An	21.2	22.2	23.3	18.6	27.0	23.4	24.3	22.6	23.3	23.9	22.6	23.7	23.4	21.5	22.5	23.2	28.3	23.7
Di	15.6	3.8	3.5	8.5	4.1	2.7	1.9	2.8	2.3	2.1	2.8	2.5	1.0	0.0	0.0	3.1	9.9	2.8
Hy	12.3	11.7	12.3	11.9	11.1	12.5	10.8	9.9	9.8	11.2	9.1	7.4	6.0	6.3	6.3	9.9	10.9	9.9
Ol	2.2	0.0	0.0	0.0	0.0	0.0	0.0	0.0	0.0	0.0	0.0	0.0	0.0	0.0	0.0	0.0	0.0	0.0
Il	0.3	0.3	0.3	0.3	0.2	0.2	0.3	0.3	0.2	0.3	0.2	0.3	0.2	0.2	0.2	0.3	0.3	0.3
Hm	9.6	9.5	9.5	8.0	9.4	9.8	8.9	8.9	8.4	9.2	8.0	7.7	7.1	6.1	6.1	8.8	10.2	8.5
Tn	1.8	3.1	3.1	2.3	2.9	3.2	2.9	2.7	2.6	3.0	2.6	2.4	1.9	1.4	0.3	2.9	2.2	2.5
Ru	0.0	0.0	0.0	0.0	0.0	0.0	0.0	0.0	0.0	0.0	0.0	0.0	0.0	0.1	0.5	0.0	0.0	0.0
Ap	0.5	0.8	0.8	0.9	0.8	1.0	1.0	1.0	1.0	0.9	0.3	0.9	1.0	0.8	0.8	0.8	0.4	0.9

7. Conclusions

- The investigated mafic dyke displays internal chemical compositional variation ranging from (outward) basalt to (inward) andesite. This dyke was derived from calc-alkaline magma. Plagioclase, hornblende, augite, biotite are the main phase of the studied dyke.
- The investigated dyke was formed under 1-3kbr water pressure and low oxygen fugacity conditions. The concipeous Nb and Ti anomalies and LILE depletion characteristics refer to arc to back-arc basalt.
- The author assumed that fractional crystallization processes produce the chemical compositional variation trend that occurs across the studied dyke

Conflicts of interest

The author declares that she has no competing financial interests or personal relationships that could have appeared to influence this work.

Acknowledgments

The author thanks Prof Dr. Tarek Ibrahim, Geological Studies Dep. Nuclear Materials Authority, Egypt for kind help in microprobe analyses.

References

1. Balk, R., Structural behavior of the igneous rocks. Geo. Soc. Am. Mem., S: 177p. (1937).
2. Hutchinson, R.M., Structure and petrology of Enchanted Rock Batholith, Liano and Gillespie Counties. Texas. Geo. Soc. Am. Bull.67. 763-806 (1956).
3. Akaad, M.K. and El Ramly, M.F., Geological history and classification of the basement rocks of the Central Eastern Desert of Egypt. Geol. Surv. Egypt, paper No.9. 24 P. (1960).
4. Stern, R. J, Gottfried, D. and Hedge C. E., Late Precambrian rifting and crustal evolution in the northeast Desert of Egypt. Geo logy V. 12, 168 – 172 (1984).
5. Beyth, M., Stern, R.J., Altherr, R., Kröner, A., The late Precambrian Timna igneous complex, southern Israel: evidence for comagmatic-type sanukitoid monzodiorite and alkali granite magma. Lithosphere 31, 103–124 (1994).
6. El-Nisr, S.A., Moghazi, A.M., Geochemistry, petrogenesis and paleotectonic significance of dyke swarms intruding Neoproterozoic basement rocks, south Marsa Alam area, Eastern Desert, Egypt. Bull. Fac. Sci. Assuit. Univ. 30, 117–134 (2001).
7. Eyal, Y., Eyal, M., Mafic dyke swarms in the Arabian–Nubian Shield. Isr. J. Earth Sci. 36, 195–211 (1987).
8. Halpern, M., Tristan, N., Geochronology of the Arabian-Nubian Shield in southern Israel and Sinai. J. Geol. 89, 639–648 (1981).
9. Stern, R.J., Manton, W.I., Age of Feiran basement rocks, Sinai: implications for late Precambrian crustal composite dike from the North Eastern Desert of Egypt. Geol. Rundsch. 76, 325–341 (1987).
10. Stern R. J., Voegeli D.A., Geochemistry, geochronology, and petrogenesis of a Late Precambrian (=590 Ma) composite dike from the North Eastern Desert of Egypt. Geol Rundsch., 76, 325 – 341 (1987).
11. Abdel-Rahman, AM., Doig, R., The Rb–Sr geochronological evolution of the Ras Gharib segment of the northern Nubian Shield. J. Geol. Soc. London 144, 577–586 (1987).
12. Moghazi, A.M., Geochemical and radiogenic isotope studies of some basement rocks at the Kid area, southeastern Sinai, Egypt. Ph.D. Thesis, Alexandria University, 377pp (1994).
13. Schandelmeier, H., Abdel Rahman, A.M., Wipfler, E., Kuster, D., Utke, A., Matheis, G., Late Proterozoic magmatism in the Nakasib suture, Red Sea Hills, Sudan. J. Geol. Soc. London 151, 485–497 (1994).
14. Meneisy, M., Vulcanicity. In: Said, R. (Ed.), The Geology of Egypt. Balkema, Rotterdam, Netherland, 157–172 (1990).
15. Camp, V.E., Roobol, M.J., Upwelling asthenosphere beneath western Arabia and its regional implications. J. Geophys. Res. 97, 15255–15271 (1992)..
16. Friz-Töpfer, A., Geochemical characterization of Pan- African dyke swarms in southern Sinai: from continental margin to intraplate magmatism. Precamb. Res. 49, 281–300 (1991).
17. El-Sheshtawi, Y.A., Geochemistry and tectonic setting of dykes in Wadi Risasa area, southeastern Sinai, Egypt. Al-Azhar Bull. Sci. 5, 617–636 (1994).
18. Baldridge, W., Eyal, Y., Bartov, Y., Steinitz, G., Eyal, M., Miocene magmatism of Sinai related to opening of the Red Sea. Tectonophysics 197, 181–201(1991).
19. Chistyakova, S.Yu. and Latypov, R.M., Primary and Secondary Chemical Zonation in Mafic Dykes: A Case Study of the Vochelambina Dolerite Dyke, Kola Peninsula, Russia R.K. Srivastava (ed.), Dyke Swarms: Keys for Geodynamic Interpretation, DOI 10.1007/978-3-642-12496-9_30, Springer-Verlag Berlin Heidelberg (2011). .

20. Bentor, Y. K., Bogoch, R., Eyal, M. and Shimron, A., Precambrian history of Sinai Peninsula: 24'h of international Geol. Congo Canada. Abstract, 4·5 (1972).
21. Abd El Ghaffar, N.I. ,El-Bagoury, H., Ghabrial, D.,Abdelwahab ,W., Ismail, A. I. Discrimination of Neoproterozoic granitic-phases in Southern-Sinai, Egypt. Remote sensing, petrography and geochemistry, The Egyptian Journal of Remote Sensing and Space Sciences 24 (2021) 231–246.
22. Richard, L. R., MinPet: Mineralogical and Petrological Data Processing System, Version 2.02. Que´bec: MinPet Geological Software (1995).
23. Deer, W. A., Howie, R. A., and Zussman, J., An Introduction to the Rock-Forming Minerals: Longman, London 528 pp (1966).
24. Hawthorne, F. C., Crystal Chemistry of the Amphiboles. Canadian Mineralogist 21, 173-480 (1981).
25. Leake, B. E., Nomenclature of amphiboles. American Mineralogist 63, 1023-1052 (1978).
26. Leake B.E., Wooley A.R., Arps C.E.S., Birch W.D., Gilbert M.C., Grice J.D., Hawthorne F.C., Kato A., Kisch H.J., Krivovichev V.G., Linthout K., Laird J., Mandarino J.A., Maresh W.V., Nickel E.H., Rock N.M.S., Schumacher J.C., Smith D.C., Stephenson N.C.N., Ungaretti L., Whittaker E.J.W. and Youzhi G., Nomenclature of Amphiboles: Report of the Subcommittee on Amphiboles of the International Mineralogical Association, Commission on New Minerals and Mineral Names, Can. Mineral., 35, 219-246 (1997).
27. Anderson, J.L. and Smith, D.R., The effects of temperature and fO_2 the Al-in-hornblende barometer. American Mineralogist, 80, 549–559 (1995).
28. Schmidt, M.W., Amphibole composition in tonalite as a function of pressure: an experimental calibration of the Al-in-hornblende barometer.Contributions to Mineralogy and Petrology 110, 304–310 (1992).
29. Deer, W. A., Howie, R. A., and Zussman, J., An Introduction to the Rock Forming Minerals: Longman, London 528 pp (1966).
30. Middlemost, E. A. K., Naming material in the magma/igneous rock system. Earth-Sci. Rev., 37, 215-224 (1994).
31. Pearce, T. H., Gorman, B. E. and Birkett, T. C., The relationship between major elements chemistry and tectonic environment of basic and intermediate volcanic rocks. Earth Planet. Sci. Lett. 36: 121-132 (1977).
32. Pearce, J. A., Trace element characteristics of lavas from destructive plate boundaries. In: R.S. Thorpe (ed.), Orogenic Andesites and Related Rocks. Wiley and Sons, New York, 525-548 (1982).
33. Irvine, T.N. and Baragar, W.A. (1971) A guide to the chemical classification of the common volcanic rocks. Can. J. Earth Sci.,8, 523-548.
34. Pearce, J. A., A user's guide to basalt discrimination diagrams. In: Wyman, D. A. (eds) Trace Element Geochemistry of Volcanic Rocks: Applications for Massive Sulphide Exploration. Geological Association of Canada, Short Course Notes12, 79-113 (1996).
35. McDonough, W. F., and Sun S.-S., The composition of the Earth, Chem. Geol., 120, 223 – 253 (1995).
36. Ilnicki, S., Petrogenesis of continental mafic dykes from the Izera complex, arkonosze-Izera block (West Sudetes, SW Poland). Int J Earth Sci 99:745–773 (2010).
37. Hazarika. B. Malpe, D & Dongre, A., Petrogenesis of mafic dykes from the western Bastar craton of Central India and their relation to outgrowth of Columbia supercontinent. Miner Petrol 243-262 (2020).
38. Polat A., Hofmann A. W., Alteration and geochemical patterns in the 3.7–3.8 Ga Isua greenstone belt, West Greenland. Precambrian Res 126:197–218 (2003).